Article:
Wallace, Suzanne K and McKenna, Keith P (2014) Grain Boundary Controlled Electron Mobility in Polycrystalline Titanium Dioxide. Advanced materials interfaces. 1400078. ISSN: 2196-7350

https://doi.org/10.1002/admi.201400078

Grain Boundary Controlled Electron Mobility in Polycrystalline Titanium Dioxide

*Suzanne K. Wallace and Keith P. McKenna**

The trapping and mobility of electrons in nanocrystalline oxide materials underpins a diverse range of applications in areas such as solar energy generation, catalysis, gas sensing and nanoelectronics.[1–5] Grain boundaries, one of the most pervasive defects in these materials, are widely believed to be critical in controlling electron mobility but probing their effects directly has proved extremely challenging. Here, we provide atomistic insight into this important issue through first principles based modeling of the interaction of electrons with grain boundaries in TiO_2. We show that perturbations in electrostatic potential are responsible for high concentrations of strong electron trapping sites at grain boundaries which hamper electron transport between grains. However, this effect is partially ameliorated at high current densities (>0.01 $mAcm^{-2}$) as a result of a highly nonlinear trap filling effect pointing to ways to help improve the performance of materials for applications such as dye-sensitized solar cells and photocatalysts.[1–6]

Nanocrystalline oxides, encompassing both porous powders and dense ceramic materials, are a ubiquitous form of technological material. However, TiO_2 is perhaps exceptional in the incredibly wide range of applications it finds, including photocatalysts for self-cleaning glass and water splitting,[3] dye-sensitized solar cells (DSSCs) for solar energy generation,[1–6] Li-ion battery materials for energy storage[7] and resistive switching memories for low power and non-volatile data storage.[5] Key to the performance of these varied applications is the transport of electrons which may be introduced by optical excitation, electrical injection or doping. For example, in catalytic applications the polaronic trapping of electrons at TiO_2 surfaces produces highly reactive Ti^{3+} sites which can facilitate chemical reactions. In DSSCs, electrons injected into the nanocrystalline network from photo-excited dye molecules must percolate through the TiO_2 network in order for electrons to reach the charge collection electrode. It has been suggested that interfaces between nanocrystals may present deep electron traps hindering electron diffusion.[1,8–10] On the other hand, enhanced electron diffusion along extended defects in resistive switching memory devices has been proposed as essential to the switching mechanism.[5] Despite its importance for these numerous applications definitive information on the electron trapping properties of grain boundaries in TiO_2 is still lacking.

First principles theoretical calculations can be invaluable to provide insight into electron trapping effects in oxide materials.[11–13] Many theoretical investigations performed within the framework of density functional theory (DFT) have studied electron trapping in TiO_2, including bulk crystals (both rutile and anatase polymorphs), surfaces and point defects.[11,12,14] These calculations are extremely challenging but accurate prediction of electron trapping can be achieved using methods such as hybrid-DFT and DFT+U which correct the self-interaction (SI) error which can lead to artificial electron delocalization (e.g. see ref. [15]). For example, it has been shown that electrons can become self-trapped at Ti ions in the rutile crystal forming small polarons consistent with experimental evidence.[12,16] At surfaces and near oxygen vacancies multiple configurations of trapped electrons can have similar stability and dynamic hopping between sites has been predicted.[17] On the other hand, electron trapping in the anatase crystal is much weaker explaining its much higher electron mobility. Surprisingly there have been no studies of electron trapping near intrinsic interfacial defects such as grain boundaries which are always present in nanocrystalline TiO_2. Here, we combine first principles based modeling with a kinetic Monte Carlo (KMC) simulation in order to investigate the effect of grain boundaries on electron trapping and mobility. We consider a model Σ5 (210)[001] tilt grain boundary in rutile[18] and focus on the intrinsic electron trapping properties of the grain boundary without defects or impurities which is something that is very difficult to do experimentally.

Grain-boundary models have been obtained through a systematic screening of different atomic configurations using a classical interatomic potential approach[19] followed by refinement at the DFT level. DFT calculations are performed within the DFT+U formalism which corrects the SI error sufficiently to allow electron localization to be described while remaining computationally feasible for complex systems containing more than 300 atoms (full details of these calculations are available in the Methods section and Supporting Information). **Figure 1**a shows the predicted structure of the Σ5 (210)[001] tilt grain boundary in rutile which is consistent with previous transmission electron microscopy studies[18] and DFT calculations.[20] The structure exhibits a high degree of order with only a few undercoordinated Ti and O ions close to the grain boundary plane. The electrostatic potential also varies significantly near the grain boundary which can play an important role in stabilizing trapped electrons. For example, the electrostatic potential on Ti ions within 5 Å of the

S. K. Wallace, Dr. K. P. McKenna
Department of Physics
University of York
Heslington, York YO10 5DD
United Kingdom
E-mail: keith.mckenna@york.ac.uk

DOI: 10.1002/admi.201400078

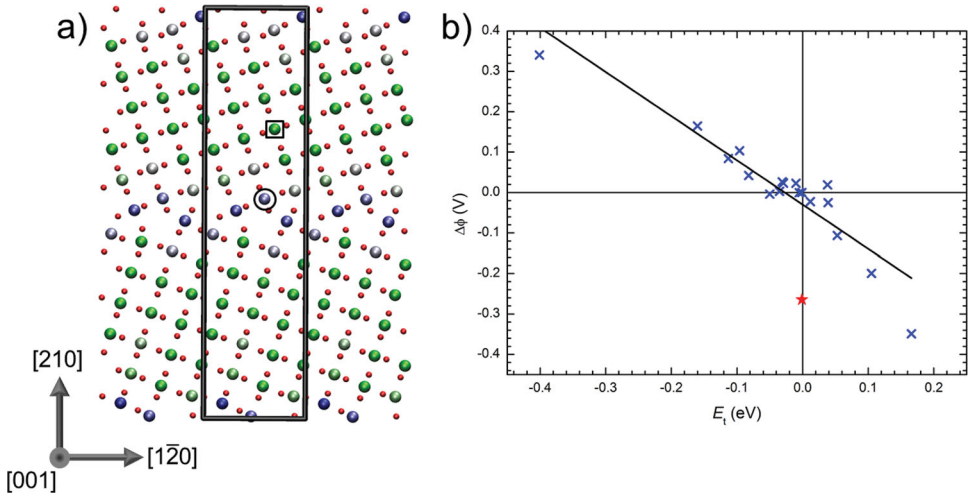

Figure 1. Predicted atomic structure of the Σ5 (210)[001] grain boundary in rutile. a) Periodic supercell (gray outline) containing two grain boundaries (one in the center of the image and one bridging the upper and lower edges). Additional periodic images of the supercell are shown in the figure to aid visualization. Large spheres represent Ti ions colored according to the magnitude of the on-site electrostatic potential (low=green, high=blue). Small red spheres represent oxygen ions. b) Correlation between the difference in on-site electrostatic potential with respect to the bulk ($\Delta\phi$) and the electron trapping energy (E_t). An almost linear correlation is found for all sites except one (red star) which is considerably more stable than should be expected given its electrostatic potential as it is coordinated to two undercoordinated oxygen atoms affording greater freedom for ion distortion on electron trapping.

grain boundary varies between ±0.35 V of the bulk potential. While the boundary considered here represents a specific case it shares common features that are observed in more general grain boundaries in a range of materials, namely undercoordination, topological disruption and strain.[21–23]

To investigate the interaction of electrons with the grain boundary defect we attempted to localize an electron polaron at all inequivalent Ti sites within 1 nm of the grain boundary plane. This involved creating a precursor potential well for electron trapping by displacing nearest neighbor anions away from a particular Ti site by 0.1 Å followed by full self-consistent optimization of the structure. Bader charge analysis of the optimized structures indicates that about 0.4 electrons localize on a single Ti ion with the remaining charge distributed over neighbouring ions.[24] Far away from the grain boundary plane the total energy is nearly independent of the site on which the electron is trapped corresponding to a bulk-like electron polaron. Therefore, in the following electron trapping energies, E_t, are defined relative to the bulk-like electron polaron which we take as the site which is equidistant between the two grain boundary planes (indicated by the black square in Figure 1a). We find there is a strong correlation between the calculated trapping energy and the difference in on-site electrostatic potential with respect to the bulk (Figure 1b). The almost linear correlation is found for all sites except one (indicated by the black circle in Figure 1a) which is considerably more stable than should be expected given its electrostatic potential. This discrepancy can be understood because it is coordinated to two undercoordinated oxygen atoms. The greater freedom for ion distortion this affords on electron trapping stabilizes the polaron despite the low electrostatic potential. A linear fit to the remaining points yields a slope of –1.1 ± 0.1, close to unity as would be predicted from a simple electrostatic model.

On the basis on the calculated trapping energies two prospective electron diffusion paths perpendicular to the grain boundary are identified labeled **a** and **b** in **Figure 2**a. We consider electron transfer between nearest neighbor Ti sites ([001] direction in the bulk) which has been shown to be the dominant diffusion mechanism in the bulk crystal.[12] The diabatic activation energies (ΔE_{ij}) for electron hopping between adjacent sites are estimated by linearly interpolating the between the two optimized polaron geometries to obtain potential energy surfaces corresponding to an electron localized on either of the two sites (Figure 2b). In the bulk-like region far from the grain boundary we find the diabatic barrier to electron hopping ΔE_{bulk} is about 0.3 eV consistent with previous bulk calculations.[12] Both paths **a** and **b** involve higher activation energies than in the bulk crystal therefore electron mobility will be reduced for electron transfer across the grain boundary. Parallel to the grain boundary we find barriers are increased for transport in the [12$\bar{0}$] direction but slightly decreased for transport in the [001] direction. In all cases the potential energy surfaces can be described to a good approximation as parabolas which are vertically displaced according to the site's trapping energy resulting in the following Marcus-like model for the activation energy between two sites with trapping energies E_i and E_j

$$\Delta E_{ij} = \frac{\left[\left(E_j - E_i\right) + 4\Delta E_{\text{bulk}}\right]^2}{4\Delta E_{\text{bulk}}}. \quad (1)$$

To fully assess the effect of the grain boundary on mobility we simulate the correlated electron transport of a flux of electrons across a bicrystal using a KMC approach similar to that used in previous studies of electron transport in nanocrystalline TiO_2 and hematite.[7,25] The rate of electron hopping between sites is described using the formalism of Marcus, Emin, Holstein, Austin and Mott[26] which gives the electron transfer rate in terms of the diabatic activation energies calculated above and the electronic coupling matrix elements H_{ab} (see Supporting Information for details). Two crystals of approximate

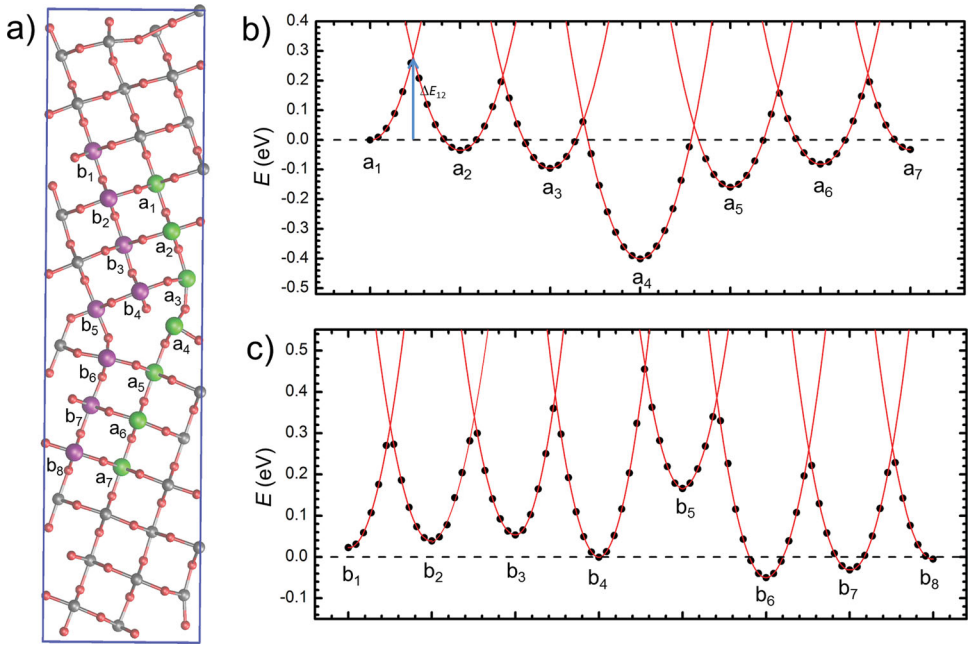

Figure 2. Potential energy surfaces for electron hopping in the vicinity of the Σ5 (210)[001] grain boundary in rutile TiO_2. a) Two possible electron diffusion paths (**a** and **b**) perpendicular to the grain boundary plane. b) Diabatic potential energy surfaces for electron hopping between Ti sites in path **a**. The points represent calculated energies while the lines are parabolas which have been fit to the calculated points nearest to the local energy minima. c) Corresponding diabatic potential energy surfaces for electron hopping between Ti sites in path **b**.

dimensions 21 × 20 × 50 Å are adjoined forming a (210)[001] grain boundary in the center as shown in in **Figure 3**. Periodic boundary conditions are employed in the directions parallel to the grain boundary and electrons are injected from the left side with a fixed rate (e.g. corresponding to photogenerated electron current). The probability for electrons to jump to unoccupied adjacent sites (in all directions) is calculated and electrons are removed from the simulation once they reach the right boundary. For calculation of the electron transfer rates we consider an adiabatic approximation (i.e. $\kappa_{el} = 1$) and take an frequency characteristic of the longitudinal optical phonon mode in rutile for ν (24 THz). The trapping energy of an electron at a given site is taken from the first principles results described above. This energy is modified by an electron-electron interaction term which depends on the locations of electrons on nearby sites. The functional form was obtained from a numerical fit to electron-electron interaction energies calculated in the bulk crystal using DFT+U. Consistent with the high dielectric constant of TiO_2 we find a highly screened Coulomb interaction which is essentially negligible beyond third nearest neighbor Ti sites. Calculation of H_{ab} is more challenging since in general it requires simultaneously accurate elimination of self-interaction error and description of the TiO_2 band gap. In the following we employ H_{ab} = 0.2 eV for nearest neighbor hopping which is a value obtained in a previous study of electron transfer in bulk rutile.[12]

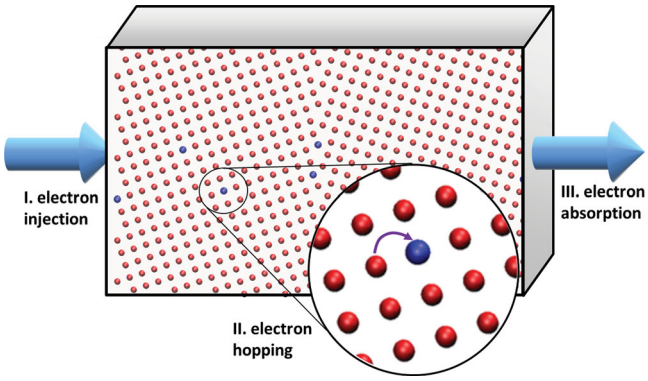

Figure 3. Overview of the kinetic Monte Carlo simulation for modeling electron transport in a TiO_2 bicrystal. Three types of process are considered: I. Injection of electrons on Ti sites on the first two atomic planes on the left. II. Electron hopping between adjacent sites. III. Absorption of electrons which reach Ti sites on the last two atomic planes on the right. Note only Ti ions are shown.

A series of KMC simulations are performed at room temperature with different electron injection rates corresponding to different current densities. After an initial transient period the system reaches a steady state where the time average of the number of electrons in the bicrystal and the net particle current is constant. To characterize the efficiency of the electron transport we calculate the electron transit time (τ) which is the average time taken for an electron to travel across the bicrystal as a function of the current density. **Figure 4** shows τ calculated for both the bicrystal cell and for a cell of equivalent crystallographic orientation but without a grain boundary (i.e. a bulk crystal) for reference. For current densities less than about 10^{-2} mAcm^{-2} the electron transit time in the presence of a single grain boundary is 7.0 ms at room temperature. This can be compared to the transit time for an equivalent distance in the bulk crystal which is 71 ns, five orders of magnitude faster. The long transit time is a result of electrons trapping at Ti sites at the grain boundary (i.e. sites $\mathbf{a}_4$ and equivalent) where they face

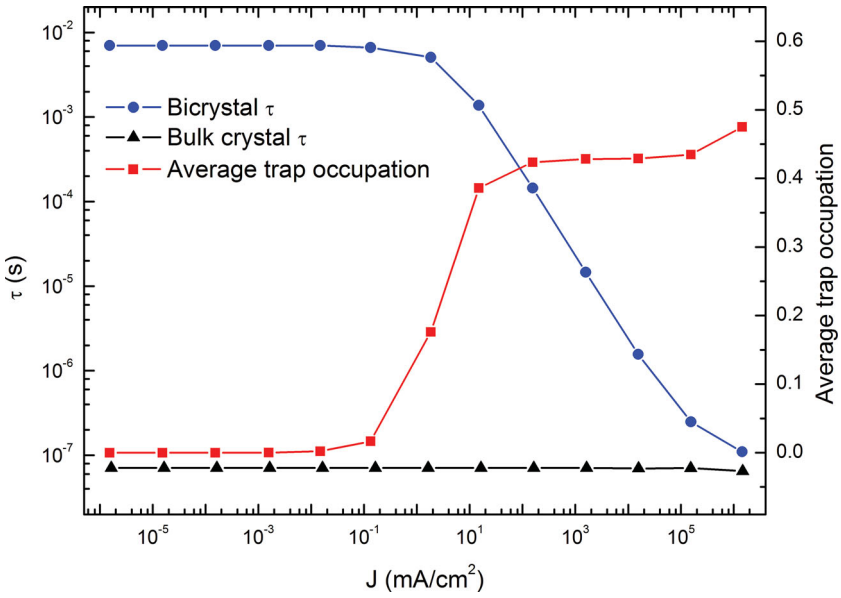

Figure 4. Dependence on the average electron transit time on the electronic current density. There is a rapid decrease in the average electron transit time (τ) for current densities greater than 10^{-2} mAcm^{-2}. The average occupation of the deepest traps (i.e. $\mathbf{a}_4$ and equivalent sites) at the grain boundary is also shown demonstrating that this effect can be explained in terms of a trap filling effect.

a high activation barrier to escape. For such low current densities the average occupation of the deepest traps at the grain boundary is very small (<0.01 electrons per site) and electron-electron interactions do not influence the transport. However, for current densities greater than 10^{-2} mAcm^{-2} the average occupation of the deepest traps at the grain boundary starts to increase. Therefore, electrons which reach the grain boundary with deep traps already filled can follow the alternate diffusion path **b** (Figure 2) which has a lower activation energy. Such a trap filling effect decreases the average residence time of electrons near the grain boundary, reducing the transit time by two orders of magnitude by 10^{2} mAcm^{-2}. Beyond 10^{2} mAcm^{-2} the occupation of the deepest traps at the grain boundary reaches it saturation point (limited by short range e-e repulsion) at about 0.4 e per site and the transit time decreases in inverse proportion to the current density up to the maximum sustainable current close to 10^{6} mAcm^{-2}.

To summarize the results, we have shown that perturbations in electrostatic potential near a grain boundary in rutile are responsible for creating Ti sites which can trap electrons more favorably than in the bulk crystal by up to 0.4 eV. As a consequence activation energies for electron diffusion are increased by up to 50% significantly reducing electron mobility. For example, a single grain boundary is found to increase the time taken for an electron to travel 10 nm from 71 ns to 7 ms at room temperature, an increase of five orders of magnitude. However, for electron current densities greater than 10^{-2} mAcm^{-2} a highly nonlinear effect is observed whereby the deepest trap states are filled under steady-state conditions resulting in a greatly reduced electron transit time. These predictions are in line with earlier observations of a so-called trap filling effect in DSSCs where higher diffusion coefficients are observed for increasing light intensity.[8] Therefore, these results provide insight into the possible origin of this effect which has proved challenging to understand by experiment alone.

While we have taken the particular example of a Σ5 (210)[001] tilt grain boundary in rutile it shares many features with more general grain boundaries, i.e. strain, coordination and electrostatic perturbation. The deep traps which control the electron mobility are associated with high electrostatic potential and similar correlations between charge trapping and electrostatic potential have been reported for a range wide gap oxides such as MgO, HfO_2 and ZrO_2 suggesting that this effect is more general.[13,27] We also find deep traps are present in similar grain boundaries in anatase suggesting they may play an equally decisive role in determining electron mobility in this material (See Supporting Information). The main challenge to quantitative prediction of electron trapping and transfer is accurate description of exchange and correlation in large complex systems. The approximate methods employed here can be considered semi-quantitative in terms of the absolute trapping and activation energies however the predicted trends are more reliable. For example, different choices for parameters like H_{ab} or ΔE_{bulk} change the absolute values of electron transit times and current densities but the overall effects are qualitatively unchanged.

With the insight gained from the above results one can suggest ways in which the mobility of materials may be improved for applications such as DSSCs and photocatalysts. Since almost all interfaces will introduce deep electrons traps as a consequence of electrostatic perturbations one approach is to employ one-dimensional nanowire structures to minimize the number of interfaces electrons must cross.[28] Alternatively one can take advantage of the trap filling effect and operate devices at higher current densities, although this may have negative consequences for device stability and durability. Another approach is to introduce *n*-type dopants to provide additional carriers to fill deep traps at the grain boundaries. For some applications the strong affinity of grain boundaries towards electrons may be beneficial. TiO_2 is considered as a prospective battery electrode material and the role of grain boundaries in the correlated diffusion of electrons and Li ions could be very important, for example aiding in separation of electrons and Li ions.[7]

Nanocrystalline oxide materials are often attractive for applications due to their ultrahigh surface area but also usually contain high concentrations of interfaces. Despite much speculation clear evidence of the effects of grain boundary defects on the polaronic trapping and mobility of electrons in nanocrystalline oxides has proved difficult to obtain. The theoretical results described above provide atomistic insight into this issue for the technologically important material TiO_2 and point to ways in which the performance of materials may be improved for applications such as DSSCs and photocatalysts. More generally, polarons play an important role in effects such as

superconductivity and magnetism.[29] where materials are also usually nano- or poly-crystalline. The first principles models of the interaction of polarons with grain boundaries presented here may help deepen our fundamental understanding of these complex effects.

Methods

The most stable grain boundary structure is obtained by screening different atomic configurations using a classical interatomic potential approach implemented in the METADISE code.[19,30] The most stable structure is converted into a three-dimensionally periodic supercell containing two equivalent grain boundaries and optimized using density functional theory (DFT) as described below.

Spin polarized DFT calculations are performed using the projector augmented wave (PAW) method as implemented within the Vienna *ab initio* simulation package.[31] We use the Perdew-Burke-Ernzerhof exchange correlation functional and correct for the self-interaction error by employing a DFT+U approach. The Hubbard U parameter for the Ti 3*d*-states is taken from previous work which fitted to spectroscopic properties of surface oxygen vacancies (U_{Ti} = 4.2 eV).[11] The valence electron wavefunctions are expanded in a plane wave basis with energies up to 500 eV and structural optimization is performed until forces are less than 0.01 eV/Å. Full details of these calculations are given in the Supporting Information.

Supporting Information

Supporting Information is available from Wiley Online Library or from the author.

Acknowledgements

K.P.M. acknowledges support from EPSRC (EP/K003151) and COST Action CM1104. This work made use of the facilities of HECToR, the UK's national high-performance computing service, via our membership in the UK HPC Materials Chemistry Consortium, which is funded by EPSRC (EP/F067496 and EP/L000202). We also acknowledge the Nuffield Foundation and Institute of Physics for supporting a summer student (S.W.).

Note: The license was changed after initial publication.

Received: February 6, 2014
Revised: March 31, 2014
Published online: May 3, 2014

[1] L. M. Peter, *J. Phys. Chem. Lett.* **2011**, *2*, 1861–1867.
[2] D. Scanlon, C. Dunnill, J. Buckeridge, *Nat. Mater.* **2013**, *12*, 10–13.
[3] A. L. Linsebigler, G. Lu, J. T. Yates, *Chem. Rev.* **1995**, *95*, 735–758.
[4] N. Barsan, D. Koziej, U. Weimar, *Sensor Actuat. B-Chem.* **2007**, *121*, 18–35.
[5] R. Waser, M. Aono, *Nat. Mater.* **2007**, *6*, 833–840.
[6] B. O'Regan, M. Grätzel, *Nature* **1991**, *353*, 737–740.
[7] J. Yu, M. L. Sushko, S. Kerisit, K. M. Rosso, J. Liu, *J. Phys. Chem. Lett.* **2012**, *3*, 2076–2081.
[8] F. Cao, G. Oskam, G. J. Meyer, P. C. Searson, *J. Phys. Chem.* **1996**, *100*, 17021–17027.
[9] A. Hagfeldt, M. Grätzel, *Acc. Chem. Res.* **2000**, *33*, 269–277.
[10] K. Benkstein, *J. Phys. Chem. B* **2003**, *107*, 7759–7767.
[11] B. J. Morgan, G. W. Watson, *Surf. Sci.* **2007**, *601*, 5034–5041.
[12] N. A. Deskins, M. Dupuis, *Phys. Rev. B* **2007**, *75*, 195212.
[13] M. J. Wolf, K. P. McKenna, A. L. Shluger, *J. Phys. Chem. C* **2012**, *116*, 25888–25897.
[14] B. J. Morgan, G. W. Watson, *Phys. Rev. B* **2009**, *80*, 233102.
[15] S. Lany, A. Zunger, *Phys. Rev. B* **2010**, *81*, 205209.
[16] S. Yang, A. T. Brant, N. C. Giles, L. E. Halliburton, *Phys. Rev. B* **2013**, *87*, 125201.
[17] P. M. Kowalski, M. F. Camellone, N. N. Nair, B. Meyer, D. Marx, *Phys. Rev. Lett.* **2010**, *105*, 146405.
[18] D. J. Wallis, N. D. Browning, P. D. Nellist, S. J. Pennycook, I. Majid, Y. Liu, J. B. V. Sande, *J. Amer. Ceram. Soc.* **1997**, *80*, 499–502.
[19] M. Matsui, M. Akaogi, *Mol. Simulat.* **1991**, *6*, 239–244.
[20] I. Dawson, P. D. Bristowe, M.-H. Lee, M. C. Payne, M. D. Segall, J. A. White, *Phys. Rev. B* **1996**, *54*, 13727–13733.
[21] S.-D. Mo, W. Y. Ching, R. H. French, *J. Phys. D: Appl. Phys.* **1996**, *29*, 1761.
[22] M. Imaeda, T. Mizoguchi, Y. Sato, H. S. Lee, S. D. Findlay, N. Shibata, T. Yamamoto, Y. Ikuhara, *Phys. Rev. B* **2008**, *78*, 245320.
[23] K. P. McKenna, A. Shluger, *Phys. Rev. B* **2009**, *79*, 224116.
[24] W.E. S. Tang, G. Henkelman, *J. Phys.: Condens. Matter* **2009**, *21*, 084204.
[25] S. Kerisit, K. M. Rosso, *J. Chem.Phys.* **2007**, *127*, 124706.
[26] R. A. Marcus, *Rev. Mod. Phys.* **1993**, *65*, 599–610.
[27] P. V. Sushko, A. L. Shluger, C. R. A. Catlow, *Surf. Sci.* **2000**, *450*, 153–170.
[28] A. I. Hochbaum, P. Yang, *Chem. Rev.* **2010**, *110*, 527–546.
[29] M. S. Senn, J. P. Wright, J. P. Attfield, *Nature* **2012**, *481*, 173–176.
[30] G. W. Watson; N. H. de Leeuw, D. J. Harris, E. T. Kelsey, S. C. Parker, N. H. D. Leeuw, *J. Chem. Soc. Faraday Trans.* **1996**, *92*, 433.
[31] G. Kresse, J. Furthmüller, *Phys. Rev. B* **1996**, *54*, 11169.